A TWO-DIMENSIONAL MODEL FOR THE PRIMORDIAL NEBULA CONSTRAINED BY D/H MEASUREMENTS IN THE SOLAR SYSTEM: IMPLICATIONS FOR THE FORMATION OF GIANT PLANETS

Franck Hersant

Département de Recherche Spatiale, Unité Mixte de Recherche 8632 du Centre National de la Recherche Scientifique, Observatoire de Paris-Meudon, Place Jules Janssen, 92195 Meudon, CEDEX, France; and Unité Propre de Recherche 182 du Centre National de la Recherche Scientifique, SAp/Commissariat à l'Énergie Atomique/Saclay, L'Orme des Merisiers, 91191 Gif-sur-Yvette, France; franck.hersant@obspm.fr

Daniel Gautier

Département de Recherche Spatiale, Unité Mixte de Recherche 8632 du Centre National de la Recherche Scientifique, Observatoire de Paris-Meudon, Place Jules Janssen, 92195 Meudon, CEDEX, France; Daniel.Gautier@megasx.obspm.fr

AND

Jean-Marc Huré

Département d'Astrophysique Extragalactique et de Cosmologie, Unité Mixte de Recherche 8631 du Centre National de la Recherche Scientifique, Observatoire de Paris-Meudon, Place Jules Janssen, 92195 Meudon, CEDEX, France; and Université Paris 7 (Denis Diderot), 2 Place Jussieu, 75251 Paris, CEDEX 05, France; jean-marc.hure@obspm.fr

Received 2000 September 27; accepted 2001 January 17

ABSTRACT

Using the density and temperature profiles resulting from a two-dimensional turbulent model of the solar nebula as well as an appropriate law for the time variation of the disk accretion rate, we integrate the equation of diffusion that rules the evolution of the D/H ratio in H_2O and HCN throughout the nebula. By fitting D/H measured in LL3 meteorites and comets or inferred in proto-Uranian and proto-Neptunian ices, we constrain the parameters of the model, namely, the initial accretion rate $\dot{M}(0)$, the initial radius of the turbulent disk R_D, and the α-coefficient of turbulent viscosity, and we find $2 \times 10^{-6} < \dot{M}(0) < 10^{-5} \ M_\odot \ \mathrm{yr}^{-1}$, $12.8 < R_D < 39$ AU, and $0.006 < \alpha < 0.04$. Under the assumption that cometary cores are homogeneous, the microscopic icy grains that subsequently formed cometesimals were produced in the Uranus-Neptune region and no later than 3.5×10^5 yr. The epochs of the formation of Jupiter and Saturn cannot be lower than 0.7 and 5.7 Myr, respectively, after the formation of the Sun. Uranus and Neptune were completed after the dissipation of the nebula. The enrichment in volatiles with respect to the solar abundance measured by the *Galileo* probe in Jupiter may result from the trapping of these gases in the form of clathrate hydrates in the feeding zone of the forming planet.

Subject headings: comets: general — planets and satellites: general — solar system: formation

1. INTRODUCTION

Drouart et al. (1999) have proposed an interpretation of the deuterium enrichment in water with respect to the protosolar value, measured in LL3 meteorites, Uranus and Neptune, and in three comets originating from the cloud of Oort. This was based on a pseudo–time-dependent one-dimensional turbulent α-disk model for the solar nebula (Dubrulle 1993). Drouart et al. (1999) showed that fitting the observed deuterium enrichments constrains the evolution with time of the temperature, pressure, and density radial profiles throughout the nebula. In turn, this determines the α-viscosity parameter, initial mass, and initial disk radius of the nebula. Subsequently, Mousis et al. (2000) have demonstrated that the nebulae selected in this way also account for the D/H ratio in HCN measured in comet Hale-Bopp.

In this report, we refine previous investigations using a pseudo-evolutionary two-dimensional model that accounts for the vertical structure of the disk (Huré 2000). Moreover, we redefine the physical and chemical data used to constrain the parameters of the model. Physical constraints concern the initial mass and initial temperature profile of the nebula, as well as the time to transport the angular momentum outward to the region where Neptune formed. Chemical constraints result from the enrichment in deuterium in water with respect to the protosolar value observed

in LL3 meteorites and comets or deduced from measurements of D/H in hydrogen in Uranus and Neptune. Another constraint is based on the deuterium enrichment in HCN measured in comet Hale-Bopp. Observations must be compared with theoretical calculations of the enrichment factor of D/H in the equatorial plan of the nebula. This is obtained by integrating the equation of diffusion of deuterated species in the nebula. Constraining the models has important implications on the theory of formation of the solar system. In particular, we may evaluate the region and the epoch of formation of cometary grains. We can estimate at what time Jupiter and Saturn were completed and determine the composition of the planetesimals which accreted onto these planets. We can also examine whether Uranus and Neptune were completed prior to the dissipation of the nebula gas.

The paper is organized as follows. Section 2 is devoted to the presentation of the two-dimensional evolutionary model. In § 3, we describe the data used to constrain the model parameters. The equation of diffusion that describes the evolution of the enrichment factor f in H_2O and in HCN with respect to the protosolar value for a given nebula model is described in § 4. The nebula models that satisfy all the observational constraints are selected in § 5. Section 6 is devoted to discussions and to the cosmogonical implications of our results. We conclude in § 7.

2. THE TURBULENT α-DISK TWO-DIMENSIONAL MODEL

2.1. General Considerations: The Thin Keplerian, Quasi-static Disk

Current accretion disk models are based on the α-prescription $v = \alpha c_s H$ (Shakura & Sunyaev 1973), which defines the anomalous turbulent viscosity from dimensional grounds (c_s is the local sound speed, H is the half thickness of the disk, and α a dimensionless parameter, $\alpha \leq 1$). A subclass of these models known as "standard disk" models assumes a Keplerian rotation law, hydrostatic equilibrium, and energy balance between viscous heating and radiative losses (see Pringle 1981 for a review). The standard model widely used to model disks around T Tauri stars (e.g., Bell et al. 1997; D'Alessio et al. 1998) intrinsically fails for high accretion rates because high accretion rates make geometrically thick disks (or $H/R \gtrsim 0.1$, where R is the heliocentric distance) that cannot be Keplerian. Using power-law solutions (Huré 1998), it can be shown that the inconsistency appears as soon as $\dot{M} \gg 10^{-5}\sqrt{\alpha}\ M_\odot$ yr^{-1}. So, the earliest stages of the primordial disk involving high accretion rates cannot be properly described by the standard model. But as the Sun accretes material, the disk mass decreases in time if no external matter is injected into the disk. This assumes that the parent circumstellar envelope does not significantly modify the disk structure. According to the standard model, this means a monotonic decrease of the accretion rate. Thus, as time goes by, the disk becomes thinner and thinner and the Keplerian assumption gets rapidly justified. Following Makalkin & Dorofeyeva (1991), the accretion rate evolution would vary as a power law of time. In this paper, we use, as do Drouart et al. (1999), the law

$$\dot{M}(t) = \dot{M}(0)\left(1 + \frac{t}{t_0}\right)^{-3/2}, \qquad (1)$$

where $\dot{M}(0)$ is the accretion rate at $t = 0$. We take for the origin of time, the moment when the Sun is almost complete. We define t_0 by

$$t_0 = \left[\frac{R_D^2}{3\,v(R_D)}\right]_{t=0}, \qquad (2)$$

where R_D is the disk size. Note that the disk has time to reach a steady state if the viscous timescale $\tau_{\rm vis} \sim R_D^2/3v(R_D)$ measured at the outer edge R_D of the turbulent disk satisfies $\tau_{\rm vis} \lesssim \tau_{\dot{M}}$, where $\tau_{\dot{M}} \sim \frac{3}{2}(t_0 + t)$ is the instantaneous variation timescale of the accretion rate. The viscous timescale increases with time for two reasons: first, the disk gets colder and colder, and thinner and thinner (i.e., $v(R_D)$ decreases); second, the disk stretches out (that is, R_D increases). In practical terms, $\tau_{\rm vis}$ and $\tau_{\dot{M}}$ remain close (within a factor $\sim$2–4) but the above inequality is never verified. It means that a time-dependent simulation allowing a natural expansion of the disk under the effect of angular momentum redistribution is indeed necessary (Ruden & Pollack 1991). Such a computation is beyond the scope of this paper. Despite the nonstationary character of the disk nebula, we treat the time-dependent problem by a series of steady state solutions with accretion rates changing according to equation (1).

2.2. Physical Quantities at the Equatorial Plane via the Two-dimensional Model

Drouart et al. (1999) used a one-dimensional disk model to compute the temperature, pressure, density, and related quantities as a function of the radius and, subsequently, their temporal evolution. Let us recall that such a model is based on the "vertical averaging": vertical gradients are replaced by a finite difference equation between the equatorial plane and the disk surface and implicitly assumes a vertically homogeneous disk. For instance, the scheme for the temperature T is

$$\frac{dT}{dz} \approx \frac{T(z = H) - T(z = 0)}{H - 0} \approx -\frac{T_c}{H}, \qquad (3)$$

where $T_c \equiv T(z = 0)$ is the midplane temperature. In this paper, we use a two-dimensional model to compute the physical quantities at the disk midplane (Huré 2000). It is based on the integration of three differential equations from the top down to the midplane, given boundary conditions. In principle, a two-dimensional model aiming to compute the vertical stratification in detail is physically more relevant than the one-dimensional model. In fact, the two models are in a good agreement (Huré & Galliano 2000). As Table 1 shows, there is only a 30% maximum deviation on the midplane temperature, with the two-dimensional model involving a slightly hotter disk than the vertically averaged model. The disk is also somewhat thicker and has a slightly larger surface density. Even a small difference in thermodynamic parameters is important for elaborating thermochemical models of the nebula since they are highly sensitive to the temperature, pressure, and surface density profiles.

The global (R, z) structure is determined mainly by the central mass M, mass accretion rate $\dot{M}$, and α-viscosity parameter. We show in Figure 1 an example of temperature distribution in the region 0.1–60 AU obtained for $\alpha = 9 \times 10^{-3}$ and $\dot{M} = 5 \times 10^{-8}M_\odot$ yr^{-1} (these parameter values correspond to our nominal nebula model at $t = 0.65$ Myr; see § 5). The computations presented here systematically take into account the turbulent pressure that affects the hydrostatic equilibrium when $\alpha \gtrsim 0.1$ but neglect vertical convection, which plays only a minor role, vertical self-gravity, and illumination by the proto-Sun. From this point of view, our models involve optically thick disks and we have checked that disk irradiation has almost no effect on midplane quantities for luminosities typical of T Tauri stars.

An important input of the disk model is the law that fixes the viscous energy release between the midplane and the

TABLE 1

VALUES FOR A STANDARD DISK OBSERVED BETWEEN TWO-DIMENSIONAL AND ONE-DIMENSIONAL MODELS

Key Quantity	Ratio	Range of Values
Thickness	h_{2D}/h_{1D}	1.0–3.3
Pressure	P_{2D}/P_{1D}	1.1–1.4
Density	ρ_{2D}/ρ_{1D}	0.4–1.4
Surface density	Σ_{2D}/Σ_{1D}	0.9–1.8
Temperature	T_{2D}/T_{1D}	1.0–1.3
Optical thickness	τ_{2D}/τ_{1D}	0.3–1.9

NOTE.—Minimum and maximum values for the ratio of some key quantities in a standard disk observed between a two-dimensional model and a one-dimensional model for $\alpha = 0.01$ and for accretion rates in the range of 10^{-9}–10^{-5} $M_\odot$ yr^{-1} and over the domain 0.05–50 AU. Pressure, density, and temperature are those in the midplane of the disk (adapted from Huré & Galliano 2000).
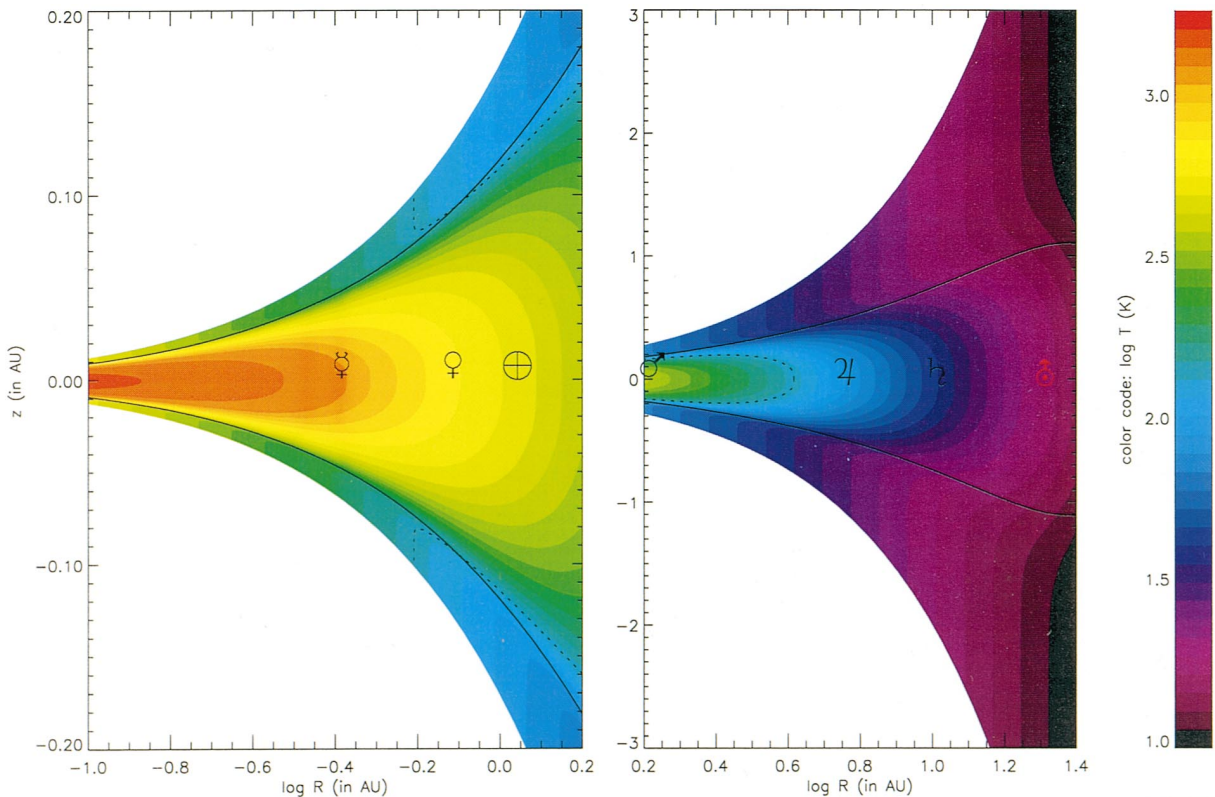
FIG. 1.—Temperature two-dimensional map in the disk for $\alpha = 9 \times 10^{-3}$ and $\dot{M} = 5 \times 10^{-8}\ M_\odot\ \mathrm{yr}^{-1}$ corresponding to the nominal solar nebula model at $t \simeq 0.65$ Myr. *Thin lines:* bottom of the disk photosphere. *Dotted line:* $T = 150$ K.

disk surface. In the present computations, we use the canonical law

$$v(z) \sim \alpha\, \frac{c_s^2(z)}{\Omega}\,, \qquad (4)$$

where Ω is the Keplerian angular velocity.

We show in Figure 2 the relationship between the accretion rate and the radius of the disk R_D for a set of iso-values of the gas mass of the disk, $M_{\mathrm{disk}}(R_D)$, defined by

$$M_{\mathrm{disk}}(R_D) = 2\pi \int_{0.01\ \mathrm{AU}}^{R_D} \Sigma(r)r\,dr\,, \qquad (5)$$

where Σ is the disk surface density. Note that Drouart et al. (1999) used M_{disk} instead of $\dot{M}$ as an input parameter. This is equivalent to our approach since the relation $M_{\mathrm{disk}}(\dot{M}, R_{\mathrm{disk}})$ can be inverted to provide a relation of the form $\dot{M}(R_{\mathrm{disk}}, M_{\mathrm{disk}})$. Very roughly, $M_{\mathrm{disk}} \propto \dot{M}^{2/3}R^{4/3}$, which is in good agreement with what can be inferred from vertically averaged models (Huré 1998).

2.3. Evolution of the Nebula: Size and Thermodynamical Structure

Under the effect of angular momentum redistribution by turbulence, the nebula spreads out with time. Accordingly, the outer radius R_D of the disk varies at a rate

$$V_R(R_D) = +\frac{3}{2}\,\frac{v}{R_D}\,, \qquad (6)$$

where v is defined by equation (4). Taking

$$V_R(R_D) \sim \frac{dR_D}{dt}\,, \qquad (7)$$

the temporal evolution of the disk outer edge is therefore governed by the equation

$$\frac{dR_D}{dt} = \frac{3}{2}\,\frac{v}{R_D}\,. \qquad (8)$$

To find $R_D(t)$, one must self-consistently solve this differential equation simultaneously with the equation $v(R, t)$ computed from the disk equation given the evolutionary law $\dot{M}(t)$. The initial radius of the nebula $R_D(0)$ is an input parameter which defines t_0 through equation (2) and constrains the subsequent evolution of the accretion rate by equation (1). An example of $R_D(t)$ is shown in Figure 3 for $\alpha = 0.009$, $\dot{M}(0) = 5 \times 10^{-6}\ M_\odot\ \mathrm{yr}^{-1}$, and $R_D(0) = 17$ AU.

Figures 4, 5, and 6, respectively, display the midplane temperature of the gas, the pressure, and disk surface density versus the radius at different epochs ranging from $t = 0$ to 5 Myr. The disk parameters (initial radius, accretion rate, and α-parameter value) are the same as for Figure 3.

3. OBSERVATIONAL CONSTRAINTS

3.1. Physical Constraints

1. *Constraints on the mass of the disk.*—The minimum initial mass of the nebula must include the mass of the heavy elements required to form the solid bodies of the solar system. Adding the mass of the gas in solar proportion results in a firm lower limit of 0.01 $M_\odot\ \mathrm{yr}^{-1}$ since we do not include the mass in this estimate, which may be substantial, of comets presently in the Oort cloud (Hahn & Malhotra 1999). To satisfy the criterion of Shu et al (1990) for the gravitational stability of the disk, the mass of the disk is limited to 0.3 $M_\odot$, whatever the time.
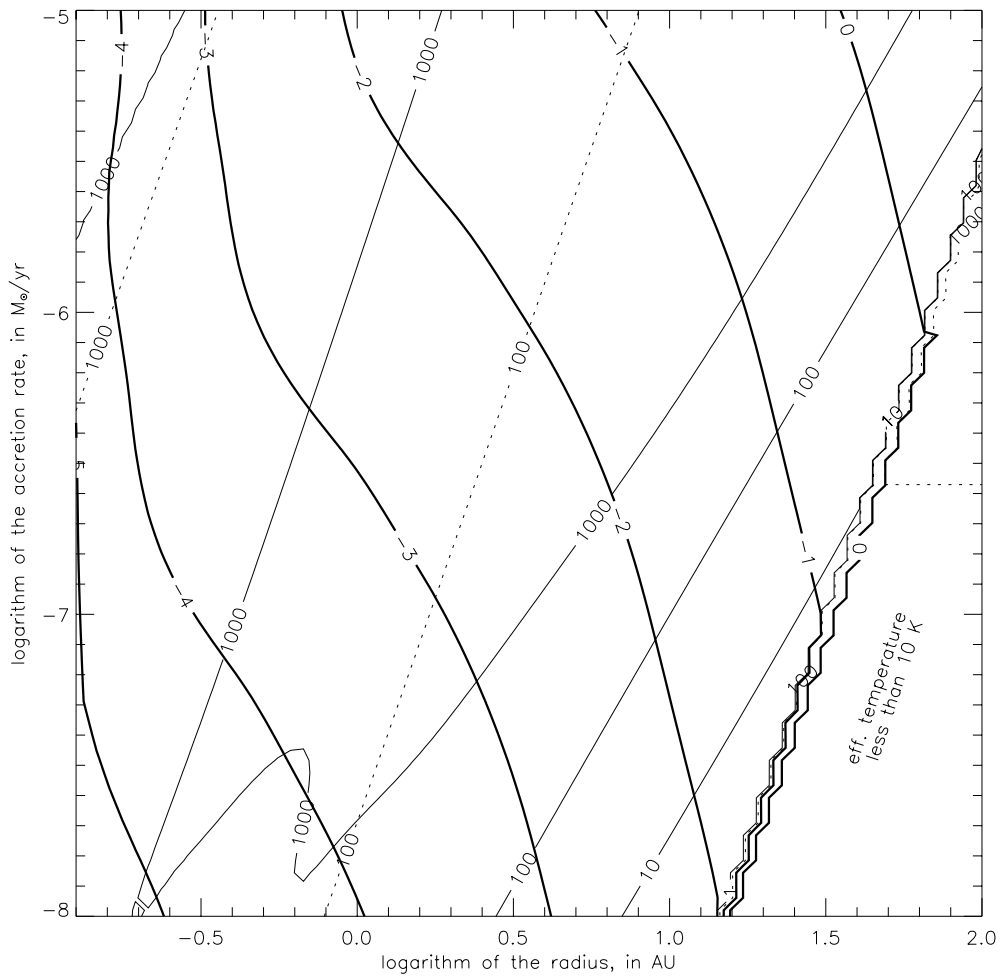
FIG. 2.—Iso-values of log $M_{disk}/M_\odot$ (*bold lines*), effective temperature (in K, *dotted lines*), and midplane temperature (in K, *thin lines*) vs. the radius and the accretion rate for $\alpha = 0.01$.

2. *Constraints from the transport of the angular momentum.*—We assume that the angular momentum must have been transported outward to the farthest giant planet, namely, Neptune, by turbulence in a time t_N and communi-

cated to microscopic grains mixed with gas. These grains, composed mainly of rocky material and ices, subsequently grew, decoupled from gas, and produced both cometesimals as well as planetesimals which formed the core of Neptune. Taking the time for the formation of microscopic cometary
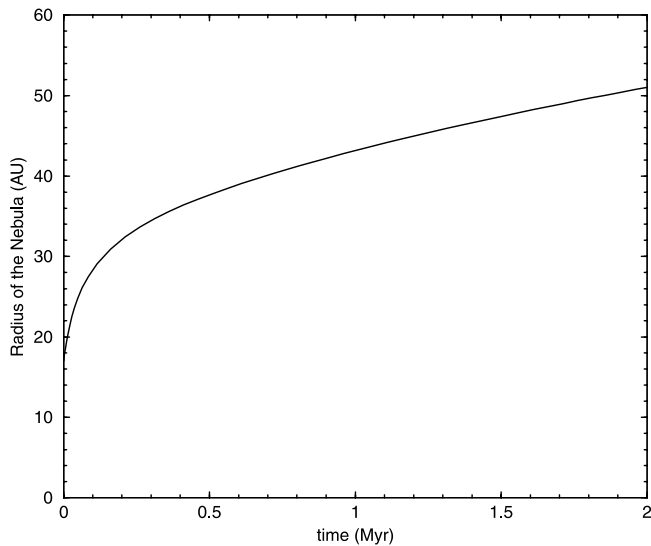
FIG. 3.—Evolution of the outer radius of the nebula with time for $\alpha = 0.009$, $\dot{M}(0) = 5 \times 10^{-6} M_\odot \, yr^{-1}$, and $R_D(0) = 17 \, AU$.
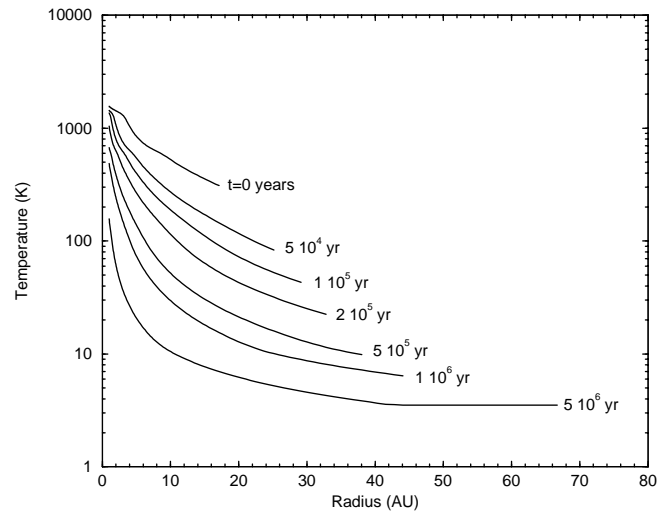
FIG. 4.—Temperature structure of the nebula at different times for $\alpha = 0.009$, $\dot{M}(0) = 5 \times 10^{-6} M_\odot \, yr^{-1}$, and $R_D = 17 \, AU$.
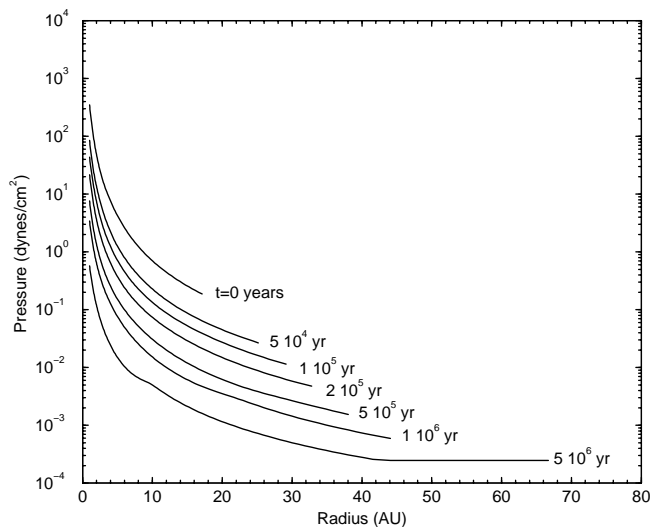
FIG. 5.—Pressure structure of the nebula at different times for $\alpha = 0.009$, $\dot{M}(0) = 5 \times 10^{-6}\ M_\odot\ \mathrm{yr}^{-1}$, and $R_D = 17\ \mathrm{AU}$.

icy grains evaluated by Mousis et al. (2000) (see also below, § 6), we adopt for t_N the value 2.5×10^5 yr. In principle, we could consider lower values and even the time $t_N = 0$, but this choice implies that one consider only nebulae for which the initial radius is at least equal to 30 AU. We will see in § 6.1 that, in this case, the range of models consistent with deuterium observations is unrealistically reduced. The case for $t_N = 500{,}000$ yr has also been tested (§ 6.1).

3. *Constraints on the temperature of the nebula.*—We assume that the initial temperature of the nebula must have been no less than 1000 K inside 3 AU. This high temperature secures the crystallization of silicates (Gail 1998) observed in meteorites and in comets. The turbulent transport of crystallized silicates from the inner nebula to the region of formation of comets and its mixing with amorphous silicates originating from the presolar cloud are discussed by Bockelée-Morvan et al. (2001).
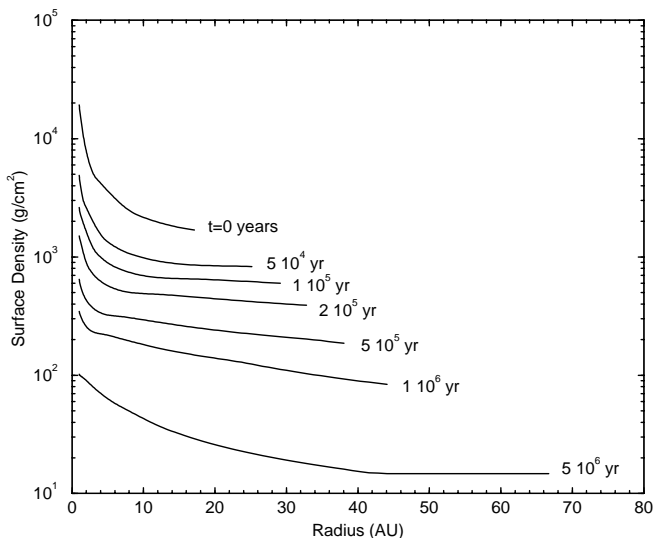

FIG. 6.—Surface density structure of the nebula at different times for $\alpha = 0.009$, $\dot{M}(0) = 5 \times 10^{-6}\ M_\odot\ \mathrm{yr}^{-1}$, and $R_D = 17\ \mathrm{AU}$.

3.2. Constraints from Deuterium Enrichments

The main reservoir of deuterium in the nebula is in hydrogen in the form of HD: the corresponding D/H ratio is named the protosolar deuterium abundance, while minor reservoirs of deuterium are in trace deuterated molecules. The deuterium enrichment observed in water constrains the temperature profile throughout the nebula (Drouart et al. 1999). At low temperatures ($T < 500$ K) deuterium tends to become heavily concentrated in H_2O, relative to H_2 (Richet, Bottinga, & Javoy 1977), so that the ratio of D/H in water to D/H in hydrogen H_2, hereafter denoted f, in primitive objects should, in principle, reveal at what temperature the enrichment occurred in the nebula. The problem is not so simple, however, since the rate of isotopic exchange between neutral molecules present in the nebula vanishes for temperatures less than 200 K. In addition, the diffusive mixing occurring in the turbulent nebula tends to smooth the gradient of the D/H ratio in the nebula. The problem can be properly solved only by integrating the equation of diffusion that governs the evolution of f as a function of the heliocentric distance R and of the time t (see § 4). This equation depends on evolutionary temperature and density profiles of the nebula. Following Drouart et al. (1999), our strategy is to calculate $f(R, t)$ from various sets of the input parameters that define the two-dimensional models described in § 1 and to compare the resulting $f(R, t)$ profiles to the enrichments observed in object relics of isotopic hydrogen exchanges that occurred in the solar nebula 4.5 billion years ago. Models that do not permit us to fit D/H observations are rejected.

The values of D/H observed in water in LL3 meteorites and in comets are shown in Figure 7, updated from Bockelée-Morvan et al. (1998), together with determinations obtained in hydrogen in giant planets. D/H values are discussed extensively in Drouart et al. (1999). However, new results have appeared since then, which deserve some comments.

1. The protosolar value of 3×10^{-5} adopted by Drouart et al. (1999) must be revised since new determinations have been published recently. First, the D/H ratio in the atmosphere of Jupiter, measured in situ by the mass spectrometer aboard the *Galileo* probe was revised by Mahaffy et al. (1998) to D/H = $(2.6 \pm 0.7) \times 10^{-5}$. Since Jupiter is made up mainly of hydrogen, the Jovian D/H ratio must be representative of the protosolar value. Second, Lellouch et al. (1997) have also inferred from *Infrared Space Observatory* (*ISO*) infrared observations of Jupiter that D/H = $(1.8^{+1.1}_{-0.5}) \times 10^{-5}$. The calibration of the *ISO* data, however, is still subject to revision. Finally, the derivation of the protosolar D/H ratio from $^3He/^4He$ measured in the solar wind has also been revised down: Geiss & Gloecker (1998) conclude to a protosolar D/H ratio of $(2.1 \pm 0.5) \times 10^{-5}$, assuming some isotopic fractionation between He in the solar wind and He at the surface of the Sun. In this work, we adopt D/H = $(2.5 \pm 0.5) \times 10^{-5}$ for the protosolar ratio. All deuterium enrichments mentioned in this paper are calculated with respect to this value.

2. The D/H ratio in water ices entering the nebula has been taken as equal to $(73 \pm 12) \times 10^{-5}$ in Drouart et al. (1999). This is the highly enriched deuterium component measured in LL3 meteorites (Deloule, Doukhan, & Robert 1998). We believe that this component originated from the presolar cloud and was never reprocessed in the nebula.
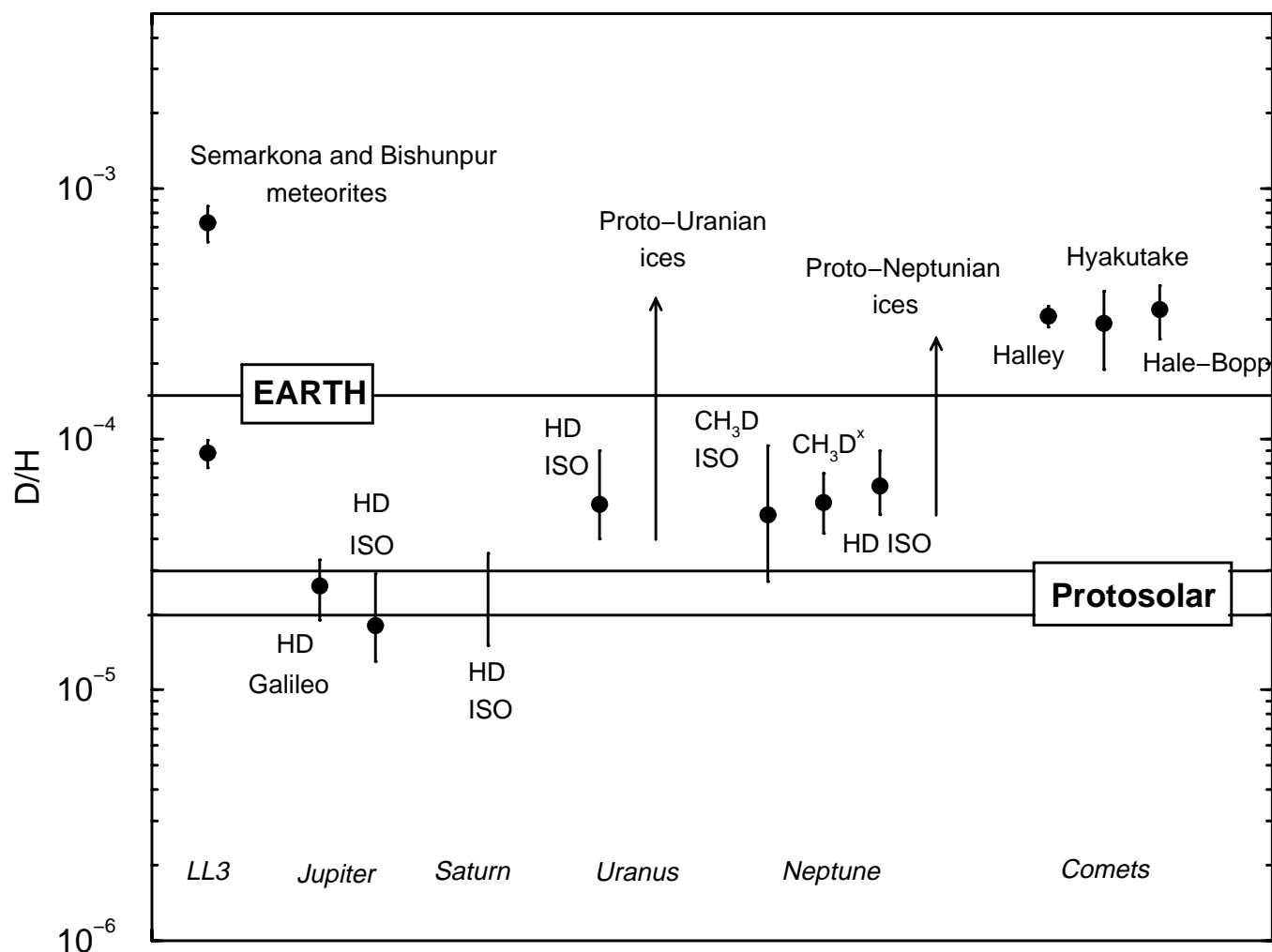
FIG. 7.—D/H ratios in the solar system. See text for explanations (updated from Bockelée-Morvan et al. 1998).

This assumption may be supported by the *ISO* detection of solid HDO in grain mantles obtained (Teixeira et al. 1999) with a corresponding D/H ratio between 40×10^{-5} and 150×10^{-5}. This range includes the value of the highly D-enriched component in LL3 meteorites. However, the reality of this detection is contested (d'Hendecourt 2000, private communication). On the other hand, the low enriched D-component measured in LL3 originates from water reprocessed in the nebula that combined with minerals around 3 AU to form clays present in the analyzed meteorites.

3. The present D/H ratio in hydrogen in Uranus and Neptune results from the mixing of the hydrogen originating from the nebula with the highly deuterium enriched ices that formed the cores of the two planets. The two components isotopically reequilibrated at high temperatures occurring in the interiors of the planets. In principle, it is possible to infer the D/H ratio in protoplanetary ices from the present D/H ratio today, provided that the relative proportions of ices and hydrogen can be estimated by models of planetary interiors. The D/H ratios in protoplanetary ices calculated by Drouart et al. (1999) from interior models available at this time (Podolak, Weizmann, & Marley 1995) were substantially less than the values in comets, suggesting that these objects have been formed at a different moment

or in a different region than Uranus and Neptune. However, new models have been published recently by Podolak, Podolak, & Marley (2000) which conclude to the possibility of a substantially higher amount of hydrogen in Uranus and Neptune than predicted by previous works. Figure 7 shows that proto-Uranian and proto-Neptunian ices exhibit D/H ratios that may be consistent with cometary values, as previously mentioned by Mousis et al (2000). This is in agreement with the current idea that cometesimals and planetesimals that formed the cores of Uranus and Neptune originated from microscopic icy grains formed at the same time and in the same region.

4. The D/H ratio has also been measured in HCN in comet Hale-Bopp (Meier et al. 1998). Using the one-dimensional model of Drouart et al. (1999), Mousis et al (2000) have shown that the models fitting D/H in H_2O in comets also fit D/H in HCN in comet Hale-Bopp. This question is reexamined using our two-dimensional model (§ 6.3).

5. Because H_2O and HCN were trapped in cometary nuclei in solid phase, we need to calculate $f(R, t)$ for each species in solid phase. In fact, there is no isotopic exchange between gas and ice, the value of f in the condensed phase is that acquired by the considered species at the time and at the heliocentric distance where it condensed.

From all these considerations, the following constraints have been imposed:

1. $f(R, t)$ calculated by integrating the equation of diffusion from the two-dimensional model must fit at some point the low D-enriched component of LL3, supposed to be formed at 3 AU, namely, the condition $2.5 < f(3\,\mathrm{AU}) < 5$ must be fulfilled.

2. A posteriori, we verify that $f(R, t)$ fits, *in solid phase*, somewhere in the turbulent nebula and, at some epoch, the enrichment measured in H_2O in the three observed comets and in HCN in comet Hale-Bopp. For H_2O, we must have $8 < f_{H_2O}(R, t) < 19$, and for HCN, $63 < f_{HCN}(R, t) < 135$.

4. EQUATION OF DIFFUSION

In the vapor phase, the derivative of $f(R, t)$ may be expressed as the sum of two terms: the first one describes the isotopic exchange between HD and the concerned deuterated molecule, here, namely, either H_2O or HCN (Lécluse & Robert 1994); the second term describes the diffusion in the nebula.

Let us examine first the diffusion term. Each species is characterized by a mixing ratio C with respect to H_2, which follows the diffusion equation

$$\partial_t C + V_R \partial_R C = \frac{1}{\Sigma R}\,\partial_R(R\Sigma\kappa\partial_R C)\,,\qquad(9)$$

where V_R is the radial velocity given by $V_R = -3/2(v/R)$, and κ is the turbulent diffusivity. The turbulent diffusivity represents the advection of matter by the small scales of turbulence and is related to the turbulent viscosity via the Prandtl number Pr by

$$\mathrm{Pr} = \frac{v}{\kappa} = \frac{\alpha C_s^2\,\Omega^{-1}}{\kappa}\,.\qquad(10)$$

The Prandtl number defined here presumably has a spatial dependence, as well as α. It cannot be calculated from a turbulent viscosity model. However, Dubrulle & Frisch (1991) have demonstrated that Pr cannot be higher than unity, in agreement with arguments developed by Prinn (1990). To simplify calculations, Drouart et al. (1999) have assumed values of Pr depending on the opacity of the considered region. In this work, we prefer to assume that Pr has no spatial dependence. We considered three values for the Prandtl number: Pr = 1, which results in the lower limit of the efficiency of the turbulent mixing, Pr = 0.7, and Pr = 0.176, which is the value derived from laboratory measurements of turbulent rotating flows by Lathrop, Fineberg, & Swinney (1992). The question of the choice of the value of Pr is discussed in § 6.2.

The deuterium enrichment factor is defined for H_2O by

$$f_{H_2O} = \frac{[HDO]}{[H_2O]}\frac{[H_2]}{[HD]}\qquad(11)$$

and for HCN by

$$f_{HCN} = 2\frac{[DCN]}{[HCN]}\frac{[H_2]}{[HD]}\,.\qquad(12)$$

Using a chain rule to express f from equation (9) we get

$$\partial_t f + \left(V_R - 2\kappa\frac{\partial_R[HD]}{[HD]}\right)\partial_R f = \frac{1}{\Sigma R}\,\partial_R(R\Sigma\kappa\partial_R f)\,.\qquad(13)$$

Assuming $\partial_R[HD]/[HD] \simeq \partial_R\Sigma/\Sigma$, we get an equation that depends only on Σ, T, and P. This approximation is quite acceptable since the isotopic exchange does not deplete in practice [HD], which is the main reservoir of deuterium in the nebula.

The term of isotopic exchange between HD and the considered deuterated species now has to be introduced. It is equal to (Lécluse & Robert 1994)

$$k(T)P[A(T) - f]\,,\qquad(14)$$

where $k(T)$ is the rate of isotopic exchange, P is the total pressure of gas, and $A(T)$ is the isotopic fractionation at the equilibrium. Lécluse & Robert (1994) have measured $k(T)$ in the laboratory for H_2O and CH_4 isotopic exchanges with hydrogen. This parameter drastically decreases with temperature. For instance, in the case of the HDO-H_2 exchange, $k(T)$ decreases by 5 orders of magnitude when the temperature varies from 1000 to 300 K. Since no experimental determination of $k(T)$ is available for the isotopic exchange of DCN with H_2, we used that of CH_4, with the expression revised by Lécluse et al. (1996). Mousis et al. (2000) have shown that a tenfold increase or decrease of $k(T)$ for the DCN-H_2 exchange does not significantly affect the fit of D/H in HCN in comet Hale-Bopp, considering the error bars. $A(T)$ is taken from the tabulations of Richet, Bottinga, & Javoy (1977) for both HDO/H_2O and DCN/HCN and is extrapolated for temperatures lower than 273 K.

Adding equation (14) to equation (13), we get finally

$$\partial_t f + \left(V_R - 2\kappa\frac{\partial_R\Sigma}{\Sigma}\right)\partial_R f$$
$$= \frac{1}{\Sigma R}\,\partial_R(R\Sigma\kappa\partial_R f) + k(T)P[A(T) - f]\,.\qquad(15)$$

Note that the isotopic exchange is practically zero at high temperatures, when both $A(T)$ and f are close to 1. The same situation occurs at temperatures lower than 200 K, at which point $k(T)$ vanishes to zero. In these two cases, the evolution of f is governed entirely by the diffusion processes, which tend to reduce any radial gradient of D/H ratios. This behavior becomes more and more pronounced as the nebula evolves. On the other hand, the isotopic exchange is efficient only at intermediate temperatures and tends to create or enhance radial gradients.

Another point is that initial conditions on the D/H ratio also affect the evolution of $f(R, t)$. The diffusion equation is integrated with the following boundary conditions:

$$\left(\frac{\partial f}{\partial R}\right) = 0\qquad(16)$$

both at $R = 0.01$ AU and R_D. As discussed in § 3.2, we adopt for the initial enrichment factor in deuterium the value of the highly D-enriched component of LL3 meteorites, namely,

$$f(R, t = 0) = 30\,.\qquad(17)$$

Drouart et al. (1999) have shown that it is not possible to fit D/H enhancements if the initial fractionation is null [i.e., $f(R) = 1$].

Equation (15) is valid as long as the considered species are in the vapor phase. As soon as the species condenses, no isotopic exchange occurs between the vapor phase and the

solid phase. In other words, the value of the enrichment in microscopic ices is that obtained at the time and at the location where the vapor condenses. As long as these ices do not exceed a few centimeters in size, they are well mixed with the nebula gas and are transported with it throughout the turbulent nebula (Dubrulle, Morfill, & Sterzik 1995).

5. RESULTS

5.1. D/H in H_2O and HCN

As an example, Figure 8 shows f_{H_2O} computed with the following model parameters: $\dot{M}(0) = 5 \times 10^{-6}$, $R_D = 17$ AU, $\alpha = 9 \times 10^{-3}$, and Pr = 0.7.

At heliocentric distances less than 3 AU, where the temperature of the nebula is higher than several hundred degrees during at least 100,000 yr, HDO exchanges rapidly *in vapor phase* with H_2 and reequilibrates with the protosolar value. However, after some time the isotopic exchange vanishes to zero when the temperature becomes lower than about 200 K. On the other hand, the enrichment in water of the inner region is mixed by turbulent diffusion with the enrichment in the outer region so that a plateau, with $f > 1$, is finally reached. The enrichment in water ice is indicated by dashed lines. As mentioned in § 4, no isotopic exchange of ice with hydrogen occurs. Microscopic icy grains are uniformly mixed with gas and the D/H ratio in ices keeps the value acquired at the moment and the location when and where H_2O condenses.

At high heliocentric distances, the behavior is similar except that the temperature range in which an efficient isotopic exchange occurs is much more limited in space and time. Moreover, the minimum heliocentric distance at which water condensation takes place (currently called "condensation radius of water") rapidly decreases with time; therefore, the isotopic exchange occurs closer and closer to the Sun.

The comparison of calculated D/H in ices with values observed in comets reveals important constraints; this is possible because the cometesimals that formed comets kept the D/H acquired in microscopic icy grains when they condensed. Under the assumption that the D/H ratio is homogeneous in the observed comets, the nebula model used to obtain the results of Figure 8 implies that, in order to fit the upper limit of D/H ratios measured in comet Hale-Bopp, cometary grains of water could not have formed farther than 14 AU and earlier than $t = 10^5$ yr after the formation of the Sun. To fit the lower limit of cometary D/H ratios, they could not have formed farther than 6 AU and later than $t = 3 \times 10^5$ yr. Once formed, microscopic icy grains propagate outward together with the nebula gas, grow up, and can form cometesimals at various heliocentric distances in the turbulent nebula (see § 6.3).

Water ice condenses at 3 AU at $t \sim 10^6$ yr, with an f value consistent with the low D-enrichment analyzed in clays in LL3 meteorites. This suggests that water combined with minerals present in the low D-enriched sample in LL3 meteorites later than 10^6 yr, unless water has reacted in vapor phase with minerals.

Figure 9 shows $f_{HCN}(R, t)$ obtained with the same set of model parameters. In this case, we do not know a priori the initial enrichment; it will be evaluated in § 6.3. Enrichments shown in Figure 9 result from an initial enrichment of 120. Our model implies that all the HCN ices entering the turbulent part of the nebula vaporized for $t \le 5 \times 10^4$ yr. An obvious difference with the behavior seen in Figure 8 is that D/H in HCN is much less reprocessed than D/H in H_2O, in agreement with the low value of the isotopic exchange rate between DCN and H_2 we have adopted in § 4. This results in a plateau value of $f \sim 90$ with respect to the protosolar value. HCN ices exhibiting a D/H ratio consistent with values measured in comet Hale-Bopp could not have condensed farther than $R = 24$ AU and earlier than 5×10^4 yr.

5.2. Selected Models of Nebula

We have carried out a large number of models by varying the initial accretion rate $\dot{M}(0)$ in the range 10^{-6}–10^{-5} $M_\odot$ yr^{-1} (step 2×10^{-6} $M_\odot$ yr^{-1}), the initial radius R_D between 5 and 45 AU (step of 0.2 AU), and the α-coefficient from 0.001 to 0.06. Besides, we have considered $t_N = 250,000$ and $500,000$ yr and two values of the Prandtl number, Pr = 1 and 0.7. About 200,000 models were investigated for each pair (t_N, Pr).
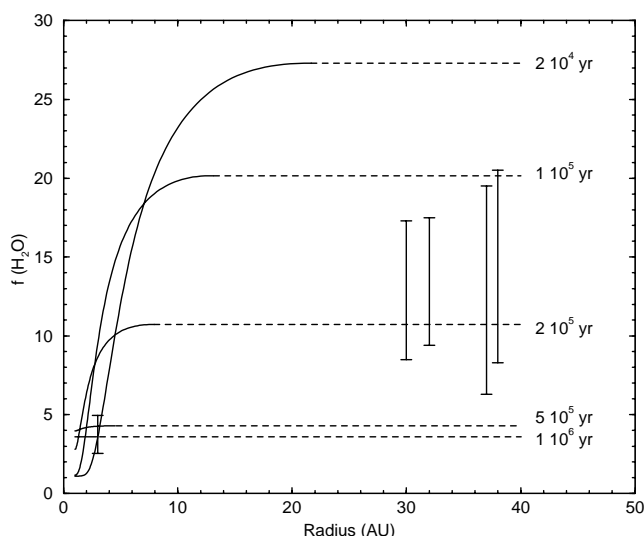
Models that did not satisfy the physical and chemical

FIG. 8.—Deuterium enrichment in H_2O fit for $\alpha = 0.009$, $\dot{M}(0) = 5 \times 10^{-6}$ $M_\odot$ yr^{-1}, and $R_D = 17$ AU.
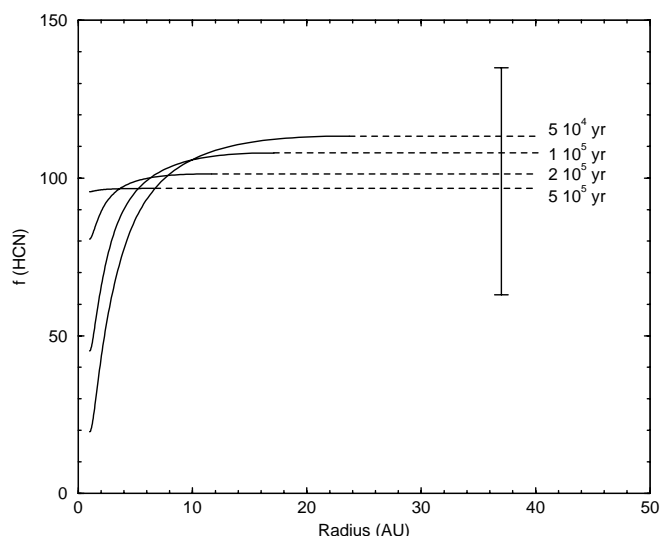
FIG. 9.—Deuterium enrichment in HCN fit for $\alpha = 0.009$, $\dot{M}(0) = 5 \times 10^{-6}$ $M_\odot$ yr^{-1}, and $R_D = 17$ AU.
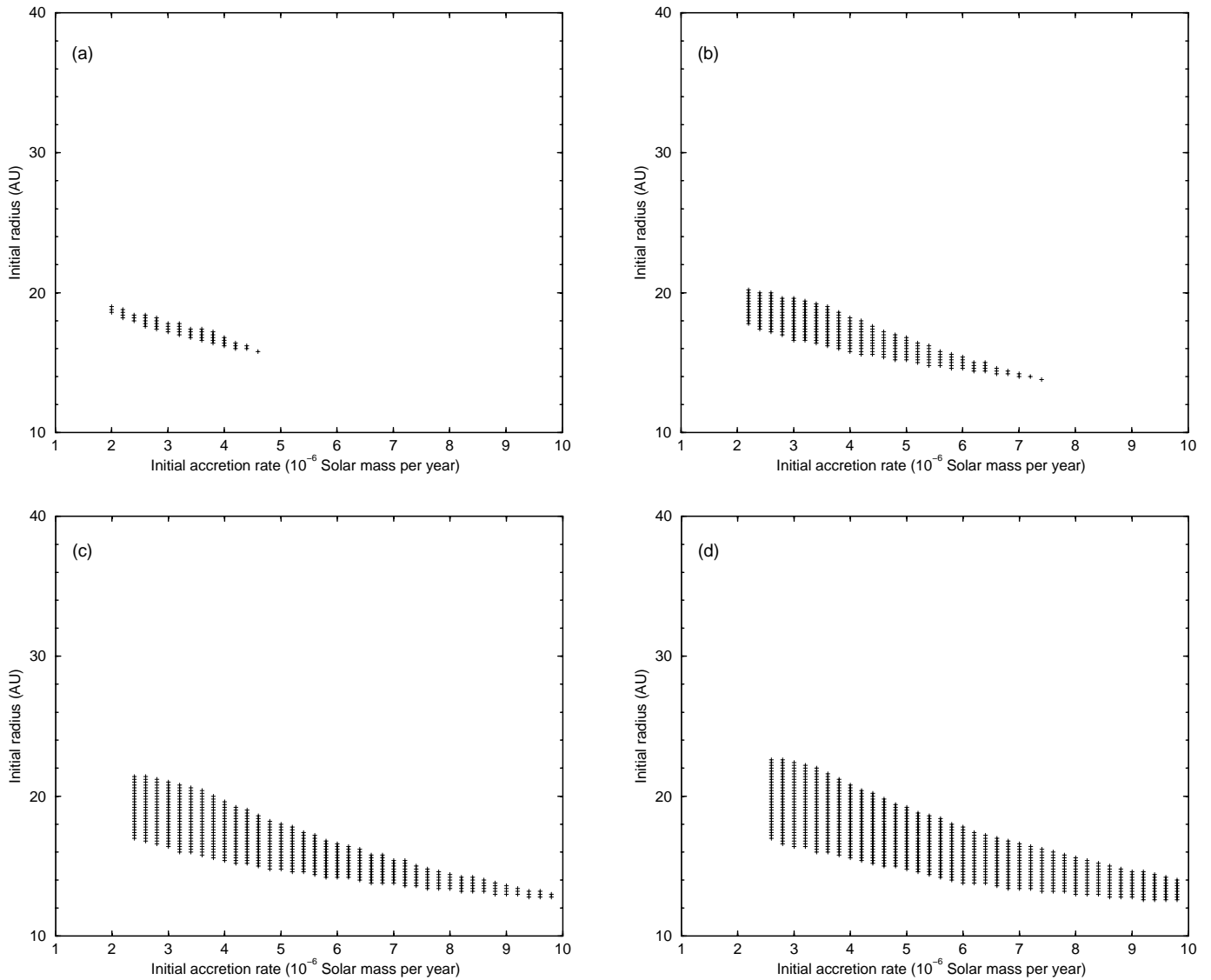
FIG. 10.—Variation of the initial radius of the selected nebulae as a function of their initial accretion rate for the following values of the α-coefficient of turbulent diffusion: (a) $\alpha = 0.006$, (b) $\alpha = 0.007$, (c) $\alpha = 0.008$, (d) $\alpha = 0.009$, (e) $\alpha = 0.01$, (f) $\alpha = 0.02$, (g) $\alpha = 0.03$, and (h) $\alpha = 0.04$. The selection of nebulae has been made for Pr = 0.7.

constraints indicated at the end of § 3 were rejected. The input parameters $[R_D(0),\ \dot{M}(0),\ \alpha]$ satisfying the required constraints are shown in Figures 10a–10h for the selected values of α: 0.006, 0.007, 0.008, 0.009, 0.01, 0.02, 0.03, and 0.04. Calculations shown on this figure were performed for $t_N = 250{,}000$ yr and Pr = 0.7.

It clearly appears that α must be between 0.006 and 0.04. The initial radius of the turbulent nebula must be between 12.8 and 39 AU. The initial accretion rates must be between 2.2×10^{-6} and 10^{-5} $M_\odot$ yr^{-1}, this upper limit being reached only for $\alpha = 0.01$. These values are consistent with those derived by Stepinski (1998) for circumstellar disks. The agreement may be fortuitous, however, considering the difficulty of precisely inferring these data parameters from observations corresponding at various ages of the disks and the large spread obtained in such determinations.

The nominal model detailed in § 2.3 appears among the possible models of Figure 10, for $\alpha = 0.009$, $\dot{M} = 5 \times 10^{-6}$ $M_\odot$ yr^{-1} and $R_D = 17$ AU. The initial mass of the disk is 0.243 $M_\odot$. For the purpose of modeling the chemistry of the

nebula, it is useful to define the "cold" and "warm" nebulae for the same t_N and Pr. For instance, these models provide upper and lower limits for the region and epoch where and when amorphous silicates are crystallized in the inner nebula (Bockelée-Morvan et al. 2001). The characteristics of the extreme nebulae compared with those of the nominal one are given in Table 2. Note that the three nebulae are initially rather massive. The warm nebula exhibits an initial mass of 0.29 $M_\odot$, close to the maximum

TABLE 2

MAIN CHARACTERISTICS OF THE COLD, NOMINAL, AND WARM NEBULAE

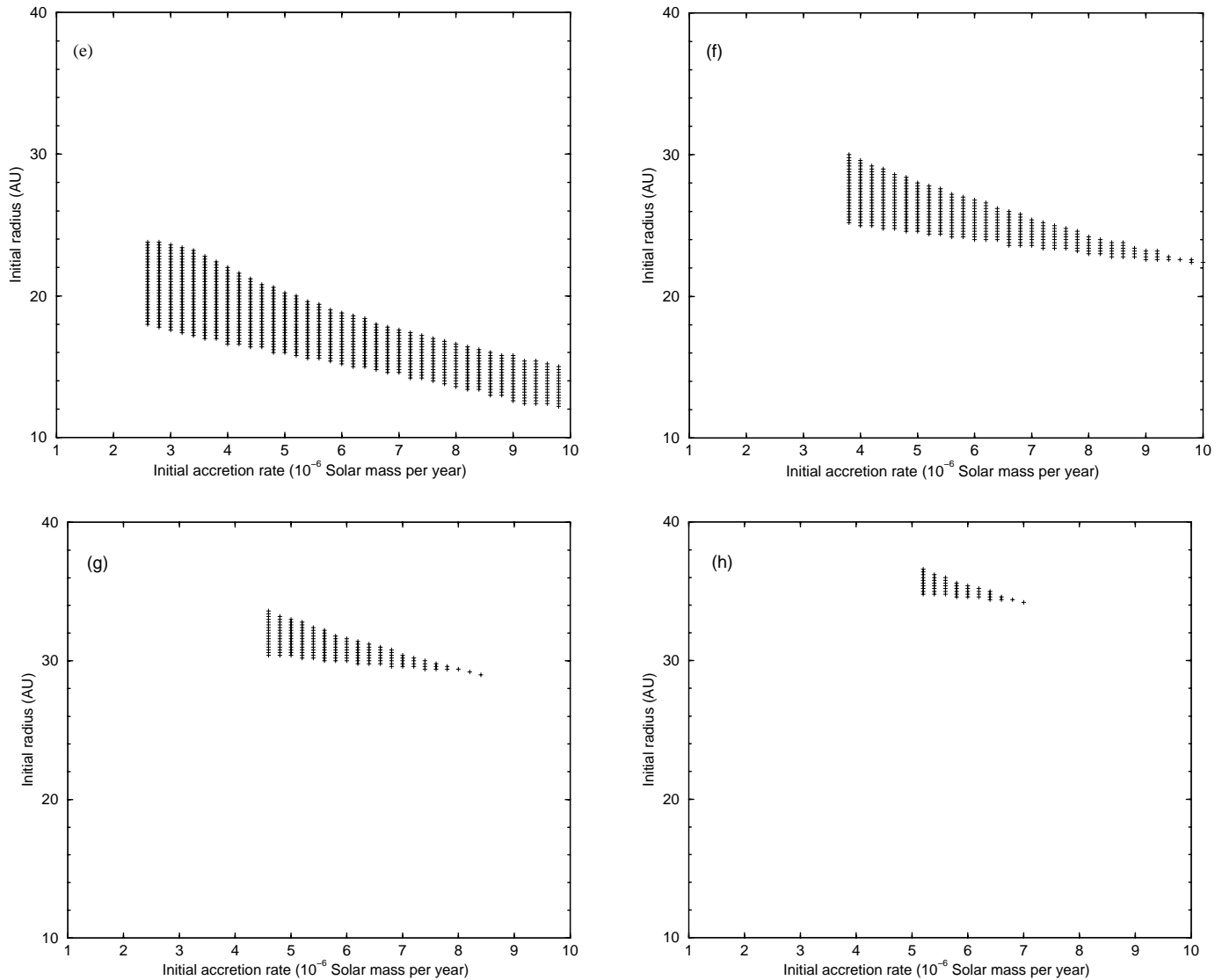| Characteristic	Cold Nebula	Nominal Nebula	Warm Nebula
α	0.02	0.009	0.008
$\dot{M}_0$	4×10^{-6}	5×10^{-6}	9.8×10^{-6}
R_D (AU)	27	17	12.8
Initial mass	0.24	0.24	0.29

FIG. 10.—*Continued*

of 0.3 $M_\odot$ permitted by the criterion of Shu et al. (1990). Note that the analysis of all selected nebulae indicates that the minimum mass required to fit D/H data is 0.15 $M_\odot$. Consequently, the so-called minimum solar nebula with $M_{disk} \sim 0.01$–0.03 $M_\odot$ is unable to match deuterium observations because it is not massive enough.

6. DISCUSSIONS

6.1. *Influence of t_N on the Selection of Models*

So far, we have presented results corresponding to the case in which the angular momentum is transported outward to 30 AU in 250,000 yr. We have also considered the case in which the angular momentum was already transported outward to the Neptune region at $t = 0$, namely, for $t_N = 0$. In this case, only values of α in the range 0.02–0.04 are compatible with the observational constraints. Actually, lower values of α would imply a disk with a mass larger than the limit of 0.3 $M_\odot$ (see § 3.1). The choice $t_N = 0$ thus appears too constrained to be wisely adopted. Interestingly enough, our selection of models is not different if we consider that Neptune was formed at 25 AU and subsequently

migrated to its current location at 30 AU (Malhotra, Duncan, & Levison 2000).

Models with $t_N = 500,000$ yr have also been considered. The results show that α must be between 0.005 and 0.04, the initial radius between 10 and 36.6 AU, and the initial accretion rate between 1.75×10^{-6} and 10^{-5} $M_\odot$ yr^{-1}. These estimates are not substantially different from the case in which $t_N = 250,000$ yr. It seems that the uncertainty on the velocity of the momentum transport does not significantly affect our results, except if the time of transport to Neptune is assumed to be quite small.

6.2. *Influence of the Prandtl Number*

The Prandtl number has a strong influence on the result of the integration of equation (15). Unfortunately, its value is uncertain. As previously mentioned, Pr cannot exceed unity (Dubrulle & Frisch 1991). We have used the same procedure for selecting models of nebula, assuming Pr = 1. The results are shown in Figure 11 where the resulting initial R_D is plotted as a function of the initial accretion rate: α must be between 0.005 and 0.007, the initial accretion rate between 1.8×10^{-6} and 2.6×10^{-6} $M_\odot$ yr^{-1}, and the initial radius R_D between 18.5 and 23 AU. The number
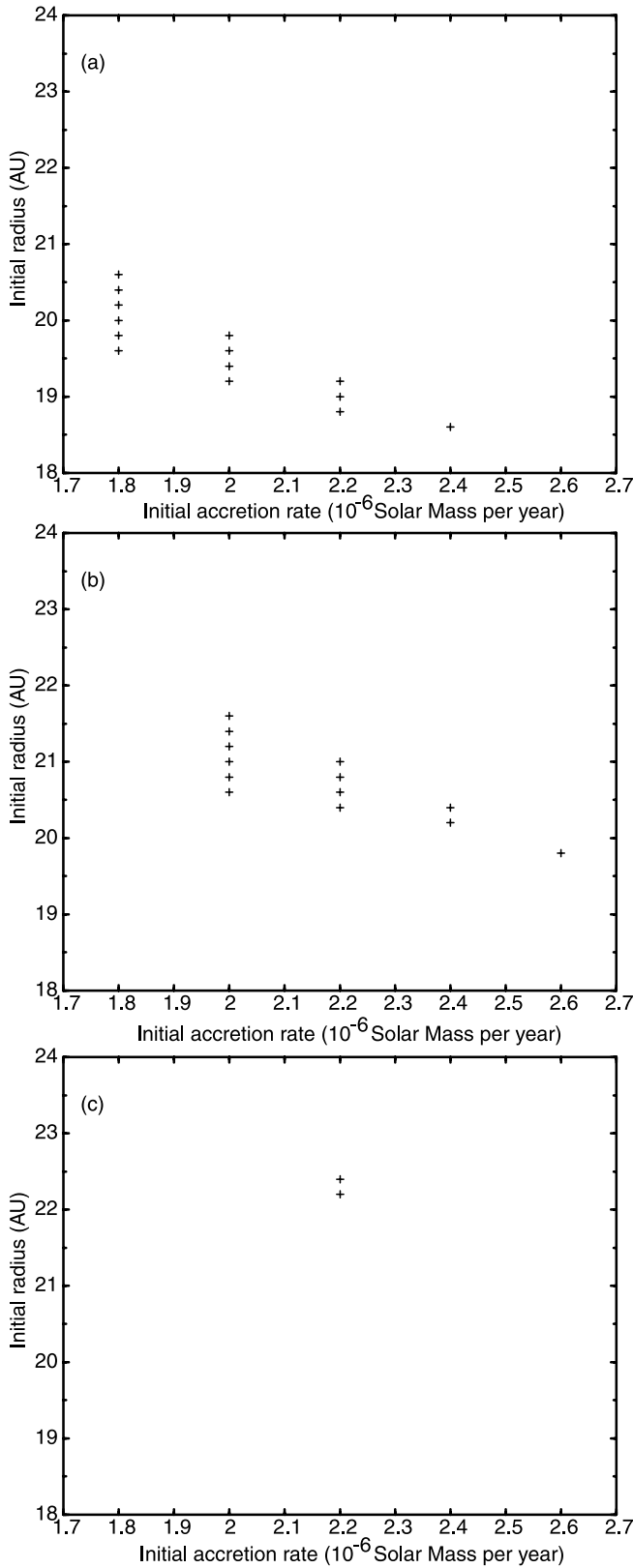
FIG. 11.—Variation of the initial radius of the selected nebulae as a function of their initial accretion rate for the following values of the α-coefficient of turbulent viscosity: (a) $\alpha = 0.005$, (b) $\alpha = 0.006$, (c) $\alpha = 0.007$. The selection of nebulae has been made for $Pr = 1$.

of possible models is much reduced compared with the case in which $Pr = 0.7$, and it would not be conservative enough to adopt this selection of models. On the other hand, adopting the value $Pr = 0.176$ measured in the laboratory by Lathrop et al. (1992) leads us to a conflict with our assumption of a geometrically thin disk model. Indeed, such a low Pr value implies very high accretion rates corresponding to geometrically thick disks. In fact, this experimental determination of Pr was made in the linearly unstable regime, namely, in the case in which the angular decreases outward, while in the nebula, it increases outward. Therefore, this Pr value is probably not applicable to the actual solar nebula.

6.3. Formation of Cometesimals in the Nebula

Using a one-dimensional model of the solar nebula, Mousis et al. (2000) determined a range of locations and epochs for the formation of cometesimals from observations. The measurements of D/H in both H_2O and HCN in comet Hale-Bopp has been used by Mousis et al. (2000) from a one-dimensional model for determining the location and the time of formation of cometesimals. Here, we follow their approach using our two-dimensional model.

Figure 12 shows the values of f_{HCN} and f_{H2O} at the heliocentric distances where HCN and H_2O respectively condensated. Calculations correspond to the nominal model and several initial HCN enrichments $f_{HCN}(R,0)$. Condensation isochrones correspond to each $f_{HCN}(R,0)$. Horizontal lines indicate the range of deuterium enrichments in HCN measured on comet Hale-Bopp. Vertical lines indicate the range of observed enrichments in water in the same comet. This procedure defines a rectangle containing acceptable values of $f_{HCN}(R,0)$. The initial deuterium enrichment in HCN then must have been between 70 and 160, which corresponds to D/H between 1.75×10^{-3} and 4×10^{-3}, in agreement with the values of the order of 3×10^{-3} found in hot cores (Schilke et al. 1992).

Interestingly enough, acceptable values of $f_{HCN}(R,0)$ are practically independent of the choice of the models selected in Figure 10. The inferred values for $f_{HCN}(R,0)$ are slightly lower than those derived by Mousis et al. (2000), which reflects the difference between their one-dimensional model and our two-dimensional model.
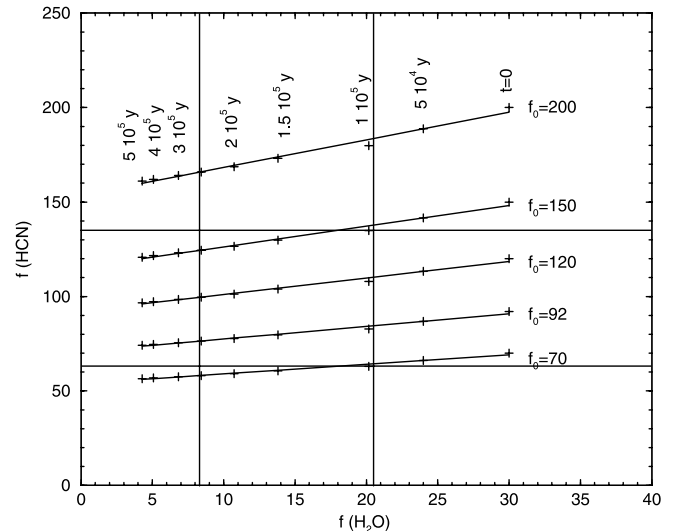

FIG. 12.—f_{H2O} with respect to f_{HCN} for $\alpha = 0.009$, $\dot{M} = 5 \times 10^{-6}\ M_{\odot}$ yr^{-1}, and $R_D(0) = 17\ AU$.
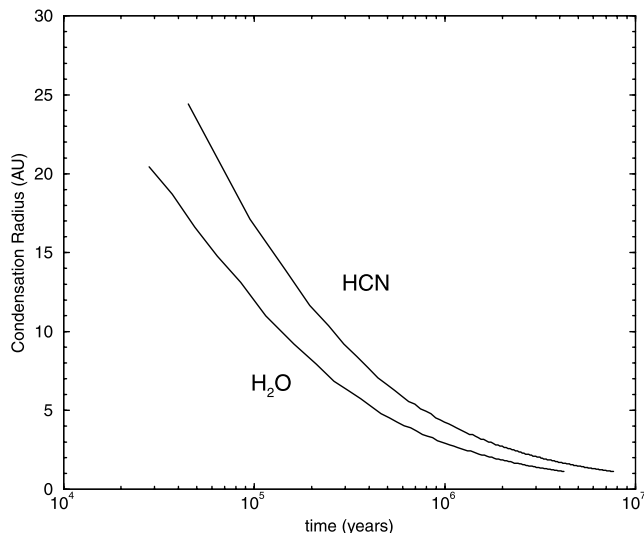
FIG. 13.—Condensation radius of H_2O and HCN with respect to time for $\alpha = 0.009$, $\dot{M} = 5 \times 10^{-6}\ M_\odot\ \mathrm{yr}^{-1}$, and $R_D(0) = 17\ \mathrm{AU}$.

FIG. 14.—Mass of gas contained within 1 AU width rings for the nominal nebula ($\dot{M} = 5 \times 10^{-6}\ M_\odot\ \mathrm{yr}^{-1}$, $\alpha = 0.009$, and $R_D(0) = 17\ \mathrm{AU}$), as a function of the heliocentric distance.

Figure 13 shows the radius of condensation of H_2O and HCN as a function of time for the nominal nebula. The range of epochs for which both the D/H ratio in both condensed H_2O and condensed HCN are consistent with comet Hale-Bopp observations are deduced from Figure 12. *Under the assumption that comets are homogeneous*, these times are 10^5 and 2.5×10^5 yr, respectively. From Figure 13, the corresponding radius of condensation for H_2O is located between 7 and 12 AU and that for HCN is between 10 and 17 AU. Ices of both species are very rapidly mixed in our selected nebulae in a time of a few ten thousand years (Bockelée-Morvan et al. 2001).

This analysis has been made for the whole set of selected models (for $t_N = 250{,}000$ yr and Pr $= 0.7$). We conclude that cometary icy grains of H_2O and HCN were formed between 18 AU at $t = 10{,}000$ yr and 7 AU at $t = 350{,}000$ yr, after the formation of the Sun. Grains moved outward with time together with gas in the expanding nebula.

Discussing the formation of comets from a swarm of microscopic particles is beyond the scope of this paper. Among an abundant literature on the question, Weidenschilling (1997) has calculated that the timescale for forming kilometer-sized comets from a uniform mixture of microscopic grains embedded in the nebula around 30 AU is less than 250,000 yr. However, he did not take into account turbulence in the disk. According to S. J. Weidenschilling (2000, private communication), introducing turbulence and continuous addition of icy grains for 350,000 yr would result in substantially longer formation times. As a result, comets could have incorporated icy grains with D/H ratios somewhat lower than the mean value presently observed. Cores of comets could be inhomogeneous and exhibit some variation in the deuterium enrichment. Present available measurements do not permit us to test this hypothesis.

We can, however, reasonably estimate that comets of the Oort cloud were formed during the first million years. The evolution of their radial repartition in the nebula during their formation is still uncertain (Stepinski & Valageas 1997). Our analysis seems at least not incompatible with the growing of the cometesimals in the Uranus-Neptune region.
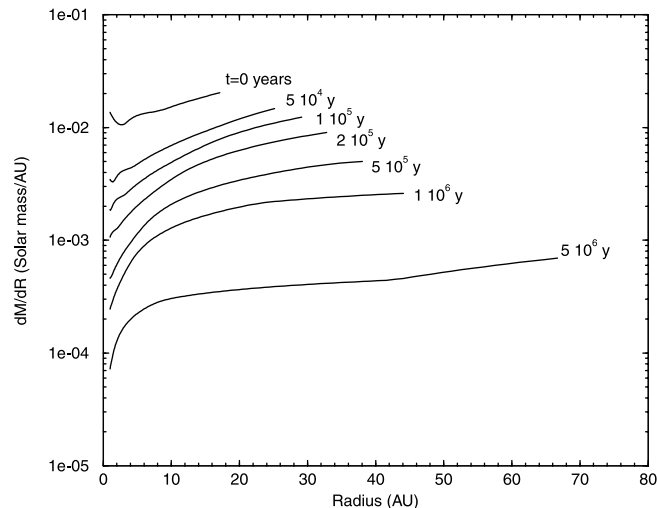
6.4. Implications on the Formation Time of the Giant Planets

6.4.1. Jupiter and Saturn

The nebula models we have calculated provide radial distributions of the gaseous mass throughout the nebula which evolve with time, as shown in Figure 14 for the nominal nebula. This figure clearly shows that most of the mass of nebula was in its outer part and, in fact, in the region where the giant planets are located today. This is because the surface density profile decreases with radius slower than $1/R$. However, the fact that Uranus and Neptune are much less massive than Jupiter and Saturn must be explained. The calculation of the temporal evolution of the mass permits us to evaluate the time of formation of giant planets based on the fact that all hydrogen currently present in these objects originated from the nebula.

This approach is based on current scenarios of the formation of giant planets (Pollack et al. 1996), which can be summarized as follows:

1. In phase 1, a core of the order of 10 Earth masses (EM) is accreted from a swarm of planetesimals in no more than 500,000 yr.

2. Phase 2 is characterized by a slow accretion of gas and planetesimals on the primary core from a region surrounding the planet and named the "feeding zone": planetesimals are supposed to be uniformly mixed in the feeding zone $2R_{FZ}$, which has sizes of 1.23 to 1.42 AU and of 1.54 to 1.74 AU for Jupiter and Saturn, respectively (Pollack et al. 1996). Note that from numerical three-dimensional simulations, A. Coradini (2000, private communication) concludes to substantially larger feeding zones. The Hill radius is 0.335 AU for Jupiter and 0.435 AU for Saturn (Pollack et al. 1996). Phase 2 continues until a critical mass of the core is reached, for which the gas of the nebula contained in the feeding zone collapses onto the core. According to Pollack et al. (1996), phase 2 for Jupiter and Saturn could have lasted between 1 and 10 millions of years.

3. Phase 3 corresponds to the hydrodynamic collapse of the nebula gas onto the core of the planet, which drastically depletes the feeding zone. This process was not modeled by

Pollack et al. (1996). The temporal evolution of the accretion during phase 3 has been developed in depth during the last years at the University of Roma using a three-dimensional hydrodynamics code. Preliminary results have been published by Coradini et al. (1995) and Forni et al. (1998). The latter conclude that the gas of the nebula collapses onto the core of Jupiter and that of Saturn in 30,000 and 20,000 yr, respectively.

The collapse of hydrogen is quasi-instantaneous compared with the duration of phase 1 and phase 2. We can thus estimate the time when Jupiter and Saturn were completed by equating their present hydrogen mass to the mass of hydrogen in the feeding zone M_{FZ}, defined at time t by

$$M_{FZ} = \int_{R_{planet} - R_{FZ}}^{R_{planet} + R_{FZ}} 2\pi R \Sigma dR . \tag{18}$$

M_{FZ} is plotted as a function of time on Figure 15 for Jupiter at 5 AU from the nominal nebula model. The complex dynamic interactions the protoplanets might have experienced with the disk are not taken into account here. In other words, no migration is considered.

The mass of hydrogen in Jupiter indicated by the horizontal line is estimated from the models of interiors of the planet recently proposed by Guillot (1999). This author concludes that the total mass of heavy elements in the interior is between 11 and 42 EM, so that the mass of hydrogen is between 276 and 307 EM. From Figure 15, we can then derive that the formation of Jupiter was completed around 1.4×10^6 yr after the formation of the Sun.

Similarly, Figure 16 shows the variation of M_{FZ} in the feeding zone of Saturn. According to Guillot (1999), the mass of heavy elements in the interior of the planet is between 19 and 31 EM. The mass of hydrogen is then between 64 and 76 EM. Figure 16 implies that, for the nominal model of nebula, Saturn was formed 1.1×10^7 yr after the formation of the Sun.

However, these results are highly dependent upon the model of nebula. We have explored the whole domain of our selected models in the prospect to determine the lower and upper limits for the time of formations of Jupiter and Saturn. The sensitive parameter in this case is the term t_0 in

FIG. 16.—Same as Fig. 15, but for Saturn with gas mass ~ 70 EM at 10 AU.

equation (1) of Makalkin & Dorofeyeva (1991), which is the characteristic time for the evolution of the nebula. The extreme values of t_0 are given in Table 3, together with the parameters of the nebula and the time of planetary formation.

From Table 3, we conclude that the formation of Jupiter was completed between 7×10^5 and 2.8×10^6 yr after the formation of the Sun. On the other hand, Saturn ended its formation between 5.7×10^6 and 2.1×10^7 yr after the formation of the Sun. The upper limit for the time of formation of Saturn creates a problem, considering the fact that most of the circumstellar disks seem to not survive after 10 Myr (Calvet, Hartmann, & Strom 2000). Around 20 Myr, the nebula may have been already dissipated by solar winds and UV solar radiation. Note also that from their model, Pollack et al. (1996) evaluate this upper limit to 10 millions of years. However, for the moment, considering uncertainties on both observations and models, we cannot firmly rule out that Saturn was completed as late as 21 millions of years after the formation of the Sun.

6.4.2. The Case of Uranus and Neptune

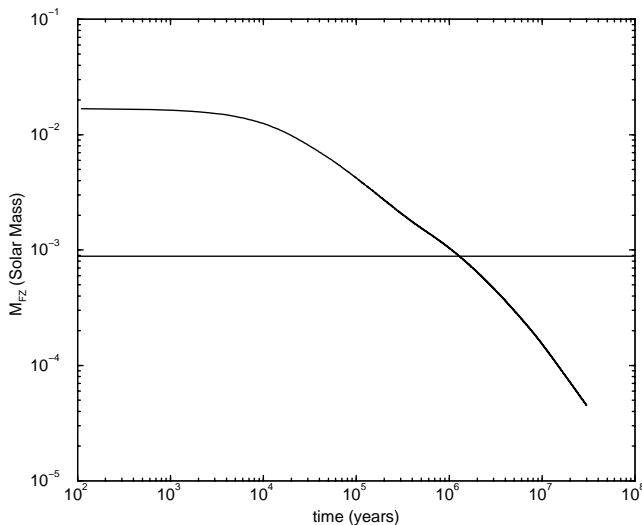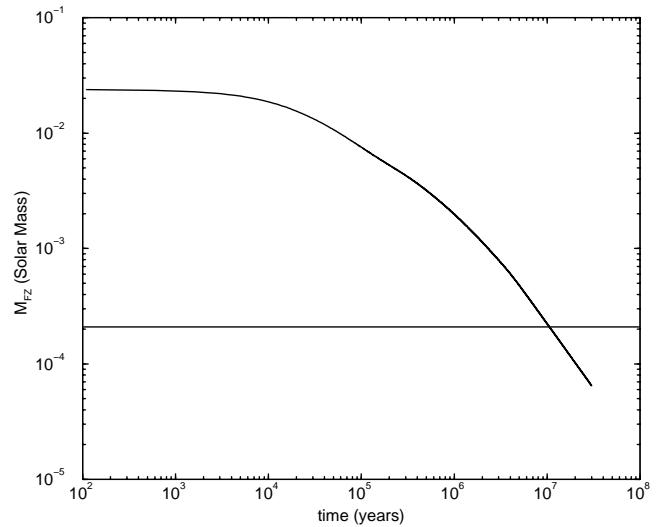It is not possible to derive the times of formation of

FIG. 15.—Total mass of gas present in the feeding zone of Jupiter, centered at 5 AU, as a function of time, for the nominal nebula. The current mean mass of Jupiter is ~ 291 EM (horizontal line; Guillot 1999).

TABLE 3

MAIN CHARACTERISTICS OF THE NEBULAE WHICH FORM JUPITER AND SATURN AT EXTREMUM TIMES

Characteristic	Minimum Value	Nominal Value	Maximum Value
α	10^{-2}	9×10^{-3}	6×10^{-3}
$\dot{M}_0$ ($M_\odot$ yr^{-1})......	9.8×10^{-6}	5×10^{-6}	2×10^{-6}
R_D (AU).............	12.2	17	19
t_0 (yr)................	12476	29853	76191
t_{jup} (yr)	7×10^5	1.3×10^6	2.8×10^6
t_{sat} (yr)...............	5.7×10^6	1.1×10^7	2.1×10^7
T_{jup} (K).............	63	55	42
T_{sat} (K)	9	8	7

NOTE.—The values t_{jup} and t_{sat} are the times of the end of Jupiter and Saturn formation, respectively, while T_{jup} and T_{sat} are the corresponding temperatures in the nebula at these times.

Uranus and Neptune by using the same approach. Indeed, even assuming a lifetime of 30 Myr for the nebula, the gas contained in the feeding zones of Uranus and Neptune when $t = 30$ Myr exceeds by a substantial factor the amount of gas present in the interiors of these planets. Podolak et al. (2000) have recently estimated that the maximum gas content for Uranus is about 4.2 EM and about 3.2 EM for Neptune. Our calculations indicate that the gas in the feeding zones of the two planets are 5 and 10 times more abundant than in Uranus and Neptune, respectively.

This result implies that the two planets never reached phase 3 of the scenario of Pollack et al. (1996). The gas present in Uranus and Neptune today was acquired during phase 2 together with accreting planetesimals. Pollack et al. (1996) indicate that, assuming infalling planetesimals of 100 m radius, the current mass of Uranus is reached in 16 millions of years. This implies that the gas of the nebula was already dissipated at this age and rules out the maximum value for Saturn indicated in Table 3.

6.4.3. Composition of Planetesimals in the Feeding Zones of Jupiter and Saturn

It is well known that the outer envelopes of the four giant planets are enriched in carbon with respect to the solar abundance (Gautier & Owen 1989). This is currently considered as being caused by the infalling of planetesimals onto the forming planet, as detailed in the scenario of Pollack et al. (1996). The question, however, is whether carbon was trapped in the form of CO or CH_4 (or both) and in what amount other volatiles were trapped. The abundance ratios for volatiles have been estimated by assuming their trapping by amorphous ice as measured at low temperature in the laboratory (Owen & Bar-Nun 1995), or their trapping in the form of clathrate hydrates, as advocated by Lunine & Stevenson (1985).

The determination of the atmospheric composition of Jupiter by the *Galileo* probe has provided new observational constraints (Folkner, Woo, & Nandi 1998; Atreya et al. 1999; Owen et al. 1999). These authors show that Ar, Kr, Xe, C, N, and S abundances relative to hydrogen are enhanced by a factor of 2 to 4 with respect to the solar abundance. This enrichment is not consistent with the trapping of ices by amorphous ice, unless one considers unconventional scenarios for the formation of Jupiter. Our evolutionary model permits us to propose an interpretation of these enrichments based on the trapping of volatiles by clathrate hydrates.

The qualitative composition of planetesimals is governed by the temperature of the condensation of their components. Solid silicates are present very early in the history of the nebula. Water ices infalling from the presolar cloud onto the nebula discoid immediately vaporized in all our models at $R < R_D$ at $t = 0$. This is the case, for instance, of the nominal model outward to 17 AU (see Fig. 4). Subsequently, the nebula cools down and H_2O condenses around 150 K. In this case, water ices are inevitably crystallized (Kouchi et al. 1994; Mousis et al. 2000). Since the saturated vapor pressure decreases extremely rapidly with temperature, most of the available H_2O gas condensed in crystalline form well above 130 K. Once formed, the crystalline ice is never converted into the amorphous variety. At much lower temperatures, the remaining H_2O gas vapor could form amorphous ice (Bar-Nun et al. 1985; Kouchi et al.
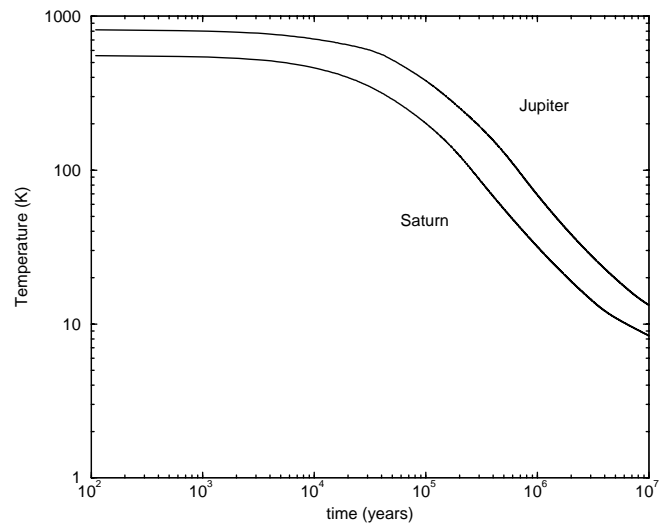
FIG. 17.—Temperatures of the nominal nebula at 5 AU (Jupiter) and 10 AU (Saturn) as a function of time.

1994) but in too small an amount to substantially trap volatiles in the way advocated by Bar-Nun et al. (1985), at least in the Jupiter-Uranus region.

Since volatiles were not trapped by amorphous ice in the feeding zones of Jupiter and Saturn, they are expected to have been trapped in the form of clathrate hydrates, as detailed below. In Figure 17, the temperature at 5 AU (Jupiter) and 10 AU (Saturn) is plotted as a function of time for the nominal model of nebula. The formation of icy grains in the feeding zone may be crudely estimated from the time when H_2O condenses, namely, at 3×10^5 yr for Jupiter and 1.3×10^5 yr for Saturn. Subsequently, icy grains grew, decoupled from gas, and produced planetesimals. The key point is that the mass of gas continuously decreases with time within the feeding zone while the mass of planetesimals tends to keep that acquired at their formation. Accordingly, the ratio of solid elements to gases continuously increases with time in this zone.

Figure 17 shows that the temperature in the feeding zones of both planets decreases rapidly and reaches values where clathrate hydrates can be formed and aggregated to planetesimals. If the time between the formation of planetesimals and the epoch of the hydrodynamic collapse of gas is substantial, planetesimals that fell onto the planet and vaporized in its envelope enriched the latter in volatiles. Temperatures in the feeding zones at the time of the collapse are given in Table 3 for the models of nebula we labeled minimum, nominal, and maximal. Let us consider, for instance, the nominal nebula, for which the collapse temperature is 55 K.

From the curves of stability of clathrate hydrates provided by O. Mousis (2000, private communication) from the analysis of Lunine & Stevenson (1985), we may evaluate, Table 4, for temperatures consistent with our model of nebula at 5 AU, the pressures at which the various volatiles are trapped in the form of hydrate $NH_3 \cdot H_2O$, clathrate hydrates of type I: $X \cdot 5.75 H_2$, or clathrate hydrates of type II: $X \cdot 5.66 H_2O$, where X is the guest molecule and the factors 5.75 and 5.66 indicate the number of water molecules per cage in the considered clathrate hydrate. The values for $CO \cdot 5.75 H_2O$, identified at the laboratory by

TABLE 4

STABILITY OF CLATHRATE HYDRATES

Clathrate Hydrate	T (K)	P (bar)
$H_2S \cdot 5.75 \, H_2O$	112	1.16×10^{-7}
$Xe \cdot 5.75 \, H_2O$	106	1.09×10^{-7}
$NH_3 \cdot H_2O$	86.5	8.8×10^{-8}
$CH_4 \cdot 5.75 \, H_2O$	77.7	7.8×10^{-8}
$Kr \cdot 5.66 \, H_2O$	73.4	7.3×10^{-8}
$CO \cdot 5.75 \, H_2O$	59.4	5.75×10^{-8}
$N_2 \cdot 5.75 \, H_2O$	59.0	5.7×10^{-8}
$Ar \cdot 5.66 \, H_2O$	54	5.13×10^{-8}

NOTE.—The factors 5.75 and 5.66 are for the ratio of the number of water molecules to the number of cages of the clathrate for type I and type II, respectively.

Davidson et al. (1987), are from J. I. Lunine (2000, private communication).

Pressures indicated in the third column of Table 4 are the minimum values required for the stability of the considered clathrate hydrate at the temperature indicated in column 2. Alternatively, the temperature indicated in the second column is the maximum value for the stability of the clathrate at the pressure indicated in column 3. For example, $CH_4 \cdot 5.75 \, H_2O$ at $T = 77.7$ K is stable at pressures higher than 7.8×10^{-8} bar. Note that the curves of stability have been extrapolated down at temperatures lower than those of laboratory measurements, which may introduce some uncertainty on the calculation.

Comparing the numbers in Table 4 with the variation of temperature at 5 AU, Figure 17, and the temperature density profile of the nominal nebula, shown in Figure 18, it then appears that H_2S, Xe, NH_3, and CH_4 should have been trapped in the form of hydrate or clathrate hydrates a long time before the collapse of the feeding zone: they were presumably incorporated in planetesimals infalling with gas onto the core of Jupiter during the hydrodynamic collapse.

On the other hand, N_2 and Ar were trapped only if the nebula was a little closer to the maximum model of Table 3. Another approach is to keep the same nebula but to

increase the width of the feeding zone. Accordingly, the mass of hydrogen in the feeding zone is larger, so that the collapse occurs at a later epoch and thus at a lower temperature. Whatever the adopted assumption, CO, N_2, and Ar were trapped at a time nearer the epoch of phase 3 than the three species mentioned above and must have been mixed mainly with hydrogen in the gaseous envelope of Jupiter. Altogether, and under the assumption that the curves of stability of clathrate hydrates are correctly extrapolated at low temperatures, this scenario provides a qualitative interpretation of the enrichment observed in Jupiter for the six elements previously mentioned (Ar, Kr, Xe, C, N, and S). We note, however, that the formation of clathrate hydrates of CO, N_2, and Ar would not have occurred in models close to the minimal nebula of Table 3, unless we adopt unrealistic large feeding zones. In the framework of our scenario, this suggests that Jupiter was completed later than 1.3 Myr after the formation of the Sun.

Estimating the resulting abundances in the gaseous envelope of Jupiter requires additional modeling, which will be the subject of a forthcoming paper (Gautier et al. 2001).

The trapping of volatiles by clathrate hydrates would be even more efficient in the case of Saturn since the temperature of the feeding zone was much lower than that of Jupiter. As a matter of fact, the temperature was so low at the time of the collapse of hydrogen (see Table 3) that all gaseous molecules, except hydrogen and helium, condensed on the grains, so that volatiles were trapped, whatever the invoked mechanism. Thus, a substantial enrichment in heavy elements must have occurred in the gaseous envelope of the planet: the enrichment, however, is presumably higher by clathration than by condensation that occurred later in the feeding zone. The atmosphere of Saturn has effectively been found enriched in carbon, phosphorus, and possibly nitrogen (Gautier & Owen 1989). Recent ground-based microwave measurements indicate that the abundance of PH_3 is 10 times solar in the deep atmosphere of the planet (Orton, Serabyn, & Lee 2000). Theoretical calculations of dissociation pressures for the PH_3 clathrate have been made by Lunine & Stevenson (1985) on the basis of laboratory measurements and suggest that PH_3 could have been trapped by this mechanism in the feeding zone of Saturn a long time before the hydrodynamic collapse of the zone, which is consistent with the high observed enrichment.

The abundance of noble gases in Saturn will unfortunately not be determined until a probe descends into the atmosphere of the planet.

7. CONCLUSION

Measurements of the D/H ratio in LL3 meteorites and comets permit us to constrain the input parameters of the evolutionary two-dimensional model we have derived from that of Huré (2000). At the time $t = 0$ of our model, namely, when the Sun is almost complete, we find that the accretion rate was between 2.2×10^{-6} and 10^{-5} $M_\odot$ yr^{-1} and the radius of the nebula was between 12.8 and 39 AU. The α-coefficient of turbulent viscosity was between 0.006 and 0.04.

These ranges are determined when assuming a value of the Prandtl number equal to 0.7 in the equation of diffusion that rules the evolution of the enrichment in deuterium in trace species throughout the nebula. The selection of nebula
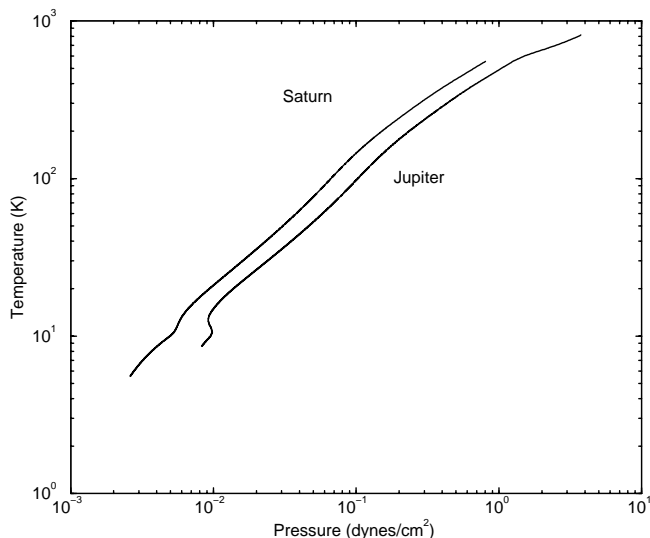

FIG. 18.—Temperature-pressure profiles of the feeding zones of Jupiter and Saturn.

models is rather sensitive to the adopted Prandtl number. We conclude from our analysis that the value Pr = 1 is unlikely, but we cannot test cases for Pr less than 0.7 since, as mentioned in § 6.2, we would have to assume that the disks are geometrically thick, which is in conflict with the basic assumption of our model. Laboratory measurements permitting an estimate of Pr in conditions applicable to the nebula would be very useful.

Under the assumption that cometary cores are homogeneous in deuterium composition, the model permits us to conclude that microscopic icy grains which subsequently formed cometesimals were produced in the Uranus-Neptune region and no later than 3.5×10^5 yr. This may provide a starting point for models of formation of cometesimals and planetesimals (see, for instance, Stepinski & Valageas 1997; Weidenschilling 1997; Supulver & Lin 2000).

Following Coradini et al. (1995), we assume that the amount of hydrogen present in the feeding zones of Jupiter and Saturn hydrodynamically collapsed onto the cores of the planets. This leads us to estimate that Jupiter and Saturn were formed between 0.7 and 2.8 Myr and 2.8 and 21 Myr, respectively. Note that the upper limit of 21 Myr is higher than current estimates of the lifetime of young stars' circumstellar disks. We emphasize that our estimate of the times of formation of Jupiter and Saturn depends on the size of the feeding zone. In this work, we have calculated this quantity from the formulas given by Pollack et al. (1996). Should the feeding zone be larger than our adopted value, as suggested by three-dimensional numerical calculations made at the University of Roma (A. Coradini 2000, private communication), the times of formation of the two planets would be increased.

This approach cannot be used for evaluating the time of formation of Uranus and Neptune because the mass of hydrogen in these planets is so small that even at 30 Myr it is much less than the mass of gas in plausible feeding zones of both planets. Therefore, we must admit that Uranus and Neptune never reached the stage of hydrodynamic collapse, and we cannot estimate their time of formation. These planets presumably accreted their hydrogen along with planetesimals onto the forming core during phase 2 of the formation in the scenario of Pollack et al. (1996). According to these authors, the present mass of Uranus was reached in no more than 16 Myr, which then would be an upper limit for the lifetime of the gaseous nebula.

Finally, our evolutionary model permits us to propose a new scenario for the composition of icy planetesimals that enriched Jupiter with respect to the solar abundance. These objects, formed in the feeding zone of the planets, progressively incorporated volatiles, trapped in the form of clathrate hydrates, when the nebula was cooling down. We emphasize that most of water vapor present in the early nebula necessarily condensed in crystalline form (Mousis et al. 2000), which then permitted the formation of clathrate hydrates. Most of the planetesimals fell with the gas into the envelope of the planet when the hydrodynamic collapse occurred. The quantitative modeling of our scenario will be the subject of a forthcoming paper.

REFERENCES

Atreya, S. K., Wong, M. H., Owen, T. C., Mahaffy, P. R., Niemann, H. B., De Pater, I., Drossart, P., & Encrenaz, T. 1999, Planet. Space Sci., 47, 1243
Bar-Nun, A., Germann, G., Laufer, D., & Rappaport, M. L. 1985, Icarus, 63, 317
Bell, K. R., Canen, P. M., Klahn, H. H., & Henning, Th. 1997, ApJ, 486, 372
Bockelée-Morvan, D., Gautier, D., Huré, J.-M., Hersant, F., & Robert, F. 2001, Icarus, submitted
Bockelée-Morvan, D., Gautier, D., Lis, D. C., Young, K., Keene, J., Phillips, T., Owen, T., Crovisier, J., Goldsmith, P. F., Bergin, E. A., Despois, D., & Wooten, A. 1998, Icarus, 133, 147
Calvet, N., Hartmann, L., & Strom, S. T. 2000, in Protostars and Planets IV, ed. V. Mannings, A. P. Boss, & S. S. Russel (Tucson: Univ. of Arizona Press), 377
Coradini, A., Federico, C., Forni, O., & Magni, G. 1995, Survey in Geophysics, 16, 533
D'Alessio, P., Canto, G., Calvet, N., & Ligano, S. 1998, ApJ, 500, 411
Davidson, D. W., Desando, M. A., Gough, S. R., Handa, Y. P., Ratcliffe, C. I., Ripmeester, J. A., & Tse, J. S. 1987, Nature, 328, 418
Deloule, E., Doukhan, J.-C., & Robert, F. 1998, Geochim. Cosmochim. Acta, 62, 3367
Drouart, A., Dubrulle, B., Gautier, D., & Robert, F. 1999, Icarus, 140, 129
Dubrulle, B. 1993, Icarus, 106, 59
Dubrulle, B., & Frisch, U. 1991, Phys. Rev. A, 43, 5355
Dubrulle, B., Morfill, G., & Sterzik, M. 1995, Icarus, 114, 237
Folkner, W. M., Woo, R., & Nandi, S. 1998, J. Geophys. Res., 103, 22847
Forni, O., Federico, C., Coradini, A., & Magni, G. 1998, in Solar System Ices, ASSL Series 227 (Dordrecht: Kluwer), 367
Gail, H.-P. 1998, A&A, 332, 1099
Gautier D., Hersant F., Mousis O., & Lunine, J. 2001, ApJ, 550, L227
Gautier, D., & Owen, T. C. 1989, in Origin and Evolution of Planetary and Satellite Atmospheres, eds. S. K. Atreya, J. Pollack, & M. S. Matthews (Tucson: Univ. of Arizona Press), 487
Geiss, J., & Gloecker, G. 1998, Space Sci. Rev., 84, 239
Guillot, T. 1999, Planet. Space Sci., 47, 1183

Hahn, J., & Malhotra, R. 1999, AJ, 117, 3041
Huré, J.-M. 1998, A&A, 337, 625
———. 2000, A&A, 358, 378
Huré, J.-M. & Galliano, F. 2000, A&A, 366, 359
Kouchi, A., Yamamoto, T., Kozasa, T., Kuroda, T., & Greenberg, J. M. 1994, A&A, 290, 1009
Lathrop, D. P., Fineberg, J., & Swinney, H. L. 1992, Phys. Rev. A, 46, 6390
Lécluse, C., & Robert, F. 1994, Geochim. Cosmochim. Acta, 58, 2297
Lécluse, C., Robert, F., Gautier, D., & Guiraud, M. 1996, Planet. Space Sci., 44, 1579
Lellouch, E., Feuchtgruber, H., de Graauw, T., Encrenaz, T., Bézard, B., & Griffin, M. 1997, A&A, in press
Lunine, J. I., & Stevenson, D. J. 1985, ApJS, 58, 493
Mahaffy, P. R., Donahue, T. M., Atreya, S. K., Owen, T. C., & Niemann, H. B. 1998, Space Sci. Rev., 84, 251
Makalkin, A. B., & Dorofeyeva, V. A. 1991, Izv. Earth Phys., 27, 650
Malhotra, R., Duncan, M. J., & Levison, H. F. 2000, in Protostars and Planets IV, ed. V. Mannings, A. P. Boss, & S. S. Russel (Tucson: Univ. of Arizona Press), 1231
Meier, R., et al. 1998, Science, 279, 1707
Mousis, O., Gautier, D., Bockelée-Morvan, D., Robert, F., Dubrulle, B., & Drouart, A. 2000, Icarus, 148, 513
Orton, G. S., Serabyn, E., & Lee, T. 2000, Icarus, 146, 48
Owen, T. & Bar-Nun, A. 1995, Icarus, 116, 215
Owen, T. C., Mahaffy, P., Niemann, H. B., Atreya, S., Donahue, T., Bar-Nun, A., De Pater, I. 1999, Nature, 402, 269
Podolak, M., Podolak, J. I., & Marley, M. S. 2000, Planet. Space Sci., 48, 143
Podolak, M., Weizman, A., & Marley, M. 1995, Planet. Space Sci., 43, 1517
Pollack, J. B., Hubickyj, O., Bodenheimer, P., Lissauer, J. J., Podolak, M., & Greenzweig, Y. 1996, Icarus, 124, 62
Pringle, J. E. 1981, ARA&A, 19, 137
Prinn, R. G. 1990, ApJ, 348, 725
Richet, P., Bottinga, Y., & Javoy, M. 1977, Annu. Rev. Earth Planet. Sci., 5, 65
Ruden, S. P., & Pollack, J. B. 1991, ApJ, 375, 740

Schilke, P., Wamsley, C. M., Pineau des Forêts, G., Roueff, E., Fower, D. R., & Guilloteau S. 1992, A&A, 256, 595
Shakura, N. I., & Sunyaev, R. A. 1973, A&A, 24, 337
Shu, F. H., Tremaine, S., Adams, F. C., & Ruden, S. P. 1990, ApJ, 358, 495
Stepinski, T. 1998, ApJ, 507, 361
Stepinski, T., & Valageas, P. 1997, A&A, 319, 1007
Supulver, K. D., & Lin D. N. C. 2000, Icarus, 146, 525
Teixeira, T. C., Devlin, J. P., Buch, V., & Emerson, J. P. 1999, A&A, 347, 19
Weidenschilling, S. J. 1997, Icarus, 127, 290